(Received 4 August 2024, Accepted 4 November 2024, Scheduled 25 November 2024)

Microwave Theremin Piano: SRR-Based Touchpad

Vladyslav Tkach[1,2], Mykola Khobzei[1,2], Serhii Haliuk[1], Ihor Safronov[1], Andrii Samila[1], Vjaceslavs Bobrovs[2], and Dmytro Vovchuk[2,*]

[1]*Department of Radio Engineering and Information Security*
Yuriy Fedkovych Chernivtsi National University, 2, Kotsyubynskyi Street, Chernivtsi 58002, Ukraine
[2]*Institute of Photonics, Electronics and Telecommunications, Riga Technical University, 6a, Kipsalas Street, LV-1048, Riga, Latvia*

ABSTRACT: Traditional touchscreens, popular for their adaptability and ease of maintenance, typically use capacitive technology where finger contact alters an electrostatic field. Here we demonstrate a touch keyboard configuration, based on a resonant-based system encompassing split-ring resonators (SRRs). These resonators, operating at the GHz spectral range, detect a finger's proximity, changing resonance frequency, but remain unaffected by distant objects — thus allowing for a parallel and independent readout of multiple keys. Specifically, 14 independent keys have been demonstrated, and the frequency-sharing protocol for parallel acquisition of sequences has been successfully implemented. The readout is performed in parallel by monitoring the transmission through a microstrip line, which is equipped with a series of distinct SRRs that resonate at different frequencies. The system has been implemented on an extremely low-cost platform, which can be transformative for similar tasks.

1. INTRODUCTION

Touch keyboards, being an alternative realization of standard worldwide used mechanical devices, keep attracting attention owing to several advantages they provide [1, 2]. Among quite a few, though subjective to the end user, worth mentioning are adaptivity, ease in maintenance, potentially longer lifetime, and a higher level of integrability within electronic circuitry. In this realm, an emphasis is put on developing touchscreen technology, which enables superimposing a context presented on a screen with user feedback. Main technologies nowadays concentrate on developing capacitive and (less common) resistive architectures [3–5]. In the capacitive approach, the sensing is based on monitoring the electromagnetic properties of activating objects like a finger. Capacitive screens have an electrode layer that creates an electrostatic field [6, 7]. When a finger touches the screen, it distorts the strong near field at that point, which is detected by sensors. More advanced realizations explore software integration, i.e., tracking the position of a finger over a screen and interpreting specific motion as an activation command [8–10].

The aim of this report is to present an alternative approach, distinct from the conventional capacitive or resistive technologies, focusing instead on a resonant-based method. Our basic element is a split-ring resonator (SRR), designed to provide a strong electromagnetic response at the GHz spectral range [11–16]. Being a resonant structure, this device is quite sensitive to the electromagnetic environment. Hence, its resonance frequency is shifted or attenuated when a dielectric object (i.e., a finger [17]) is in the vicinity [18–20]. On the other hand, the electromagnetic field is well concentrated around the resonator, which makes it less sensitive to distant objects. This compromising range makes the SRR a good candidate for implementing a touchless key — it reacts to a finger in its vicinity and is indifferent to a finger placed on a nearby key. For realizing several independent keys, SRRs with different electromagnetic parameters will be designed. In this case, we will make a spectral sharing for multiple key realizations. It should be mentioned that a concept closely resembling ours was reported recently [21, 22]. However, the concept of altering antenna impedance with dielectric objects, such as hands, has a much longer history. The theremin, created by Léon Theremin in 1920, is notable for its touchless manipulation of music through hand movements [23]. Players adjust their hands near two antennas — one controls pitch and the other volume-disrupting electromagnetic fields. These disruptions in impedance are then converted into music, using analog technology to produce its distinctive sound. The concept applied here is quite similar, utilizing the same effect to activate keys, either simultaneously or in sequence. A digital response, instead of an analog one, is implemented [24, 25]. The manuscript is organized as follows. The basic design of the single key comes first and then is followed by a detailed analysis demonstrating finger-activated scenarios. Implementation of low-cost hardware capable of managing the concept is discussed prior to the conclusion.

2. SINGLE SRR KEY --- OPTIMIZATION

Resonant elements alter their electromagnetic responses when a perturbation is introduced. Among the various architectures, we will focus on split ring resonators (SRRs) [26, 27] due to their ease of optimization and relatively high near-field confinement at the magnetic dipole resonant frequency. Specifically, a rectangular shape is chosen, with the key geometric parameters,

* Corresponding author: Dmytro Vovchuk (dimavovchuk@gmail.com).

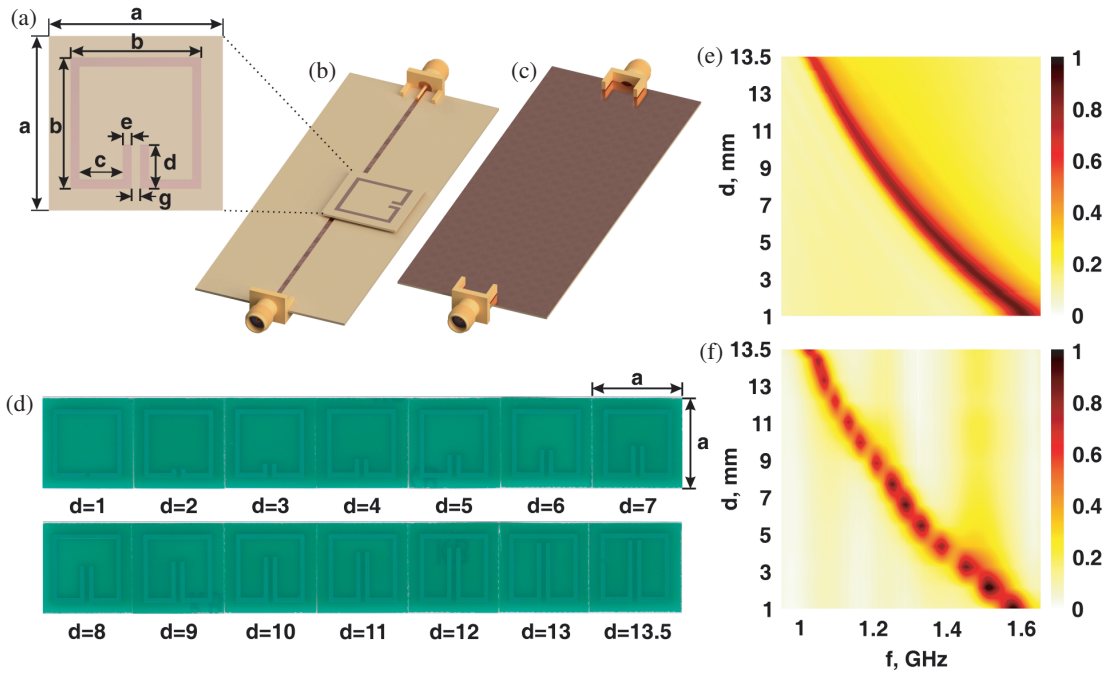

FIGURE 1. Tuning of split-ring resonators (SRRs). (a) The basic geometry of a single SRR with dimensions indicated on the plot. (b), (c) top and back views of the device, encompassing the SRR and the microstrip line for monitoring the transmission. (d) Photographs of the experimental samples. The value of the tuning parameter 'd' is indicated, the rest parameters correspond to the indicated on the panel (a). (e), (f) Colormaps, demonstrating the absolute value of the microstrip line transmission ($|S_{21}|$) as the function of frequency and the tuning parameter ('d'. (e) and (f) stay for the numerical and experimental analysis, respectively.

indicated in Fig. 1(a). Since the structure's resonant frequency is determined by its inductance and capacitance, it can be tuned by adjusting the latter property, for example. In this case, increasing 'd' will lower the resonant frequency, which approximately follows the inverse square root of this parameter.

In our implementation, unlike the typical free-space interrogation, the SRR is positioned on a transmission line, thereby altering the transmission coefficient (S_{21} parameter, if two ports of a vector network analyzer (VNA) are connected to the line input and output, respectively). The typical layout of this arrangement is schematically depicted in Figs. 1(b) and (c) for the top and bottom views, respectively. Fig. 1(d) demonstrates the range of fabricated devices, where 'd' is the only variable, changing among those 14 realizations. Those geometric parameters were optimized to grant resonances in the 1.0–1.7 GHz frequency range, which is rather arbitrary and dictated by the range of available experimental equipment. Another aspect of choosing the frequency band is the size of an activating finger, which matches quite well the characteristic dimensions. This point will be elaborated in the next section. It is worth noting that all those parameters can be adjusted along the MHz-GHz band quite straightforwardly. The rest of the parameters are: (i) superstrate (copper with thickness 0.025 mm) over the dielectric substrate (FR-4, $\varepsilon = 4.4$, $\tan(\delta) = 0.02$), (ii) transmission line: 1 mm width and 100 mm length, two 50-Ohms SMA connectors, soldered to the line. The numerical optimizations were done with the CST Microwave Studio, the frequency domain solver with the open (add space) boundary conditions.

Colormaps in Figs. 1(e) and (f) demonstrate the evolution of the resonant frequency with the changes in geometry. Each horizontal cut through those graphs is the transmission spectrum ($|S_{21}|$), measured with two ports of the transmission line. As expected, the resonance shifts to lower frequencies with increased capacitance ('d' parameter). Numerical predictions fit the experiments quite well (comparison between panels (e) and (f), respectively). The experiments were performed by connecting the N5232B PNA-L Microwave Network Analyzer (300 kHz–20 GHz) to SMA connectors on the transmission line. SRRs were glued to the substrate without introducing electrical contact. The samples were fabricated by a standard chemical etching of the copper layer.

3. SRR KEYS CASCADING --- NEAR-FIELD SCANS

It is worth noting that designing SRRs with non-overlapping resonances facilitates the implementation of the spectral-sharing protocol. This protocol enables simultaneous monitoring of disturbances, such as finger activations, across multiple elements located on the same line. Here, a single output can monitor multiple keys simultaneously. The following experiment has been performed to demonstrate the validity of this approach. The transmission line was connected to the PNA, transmitting quasi-monochromatic signals (single tones) through the device. The frequency was swept over the entire operational bandwidth of the device. The second port of the line was 50 Ω terminated to prevent back reflections. A probe (nonresonant loop) was positioned on a scanner (Midas Orbit

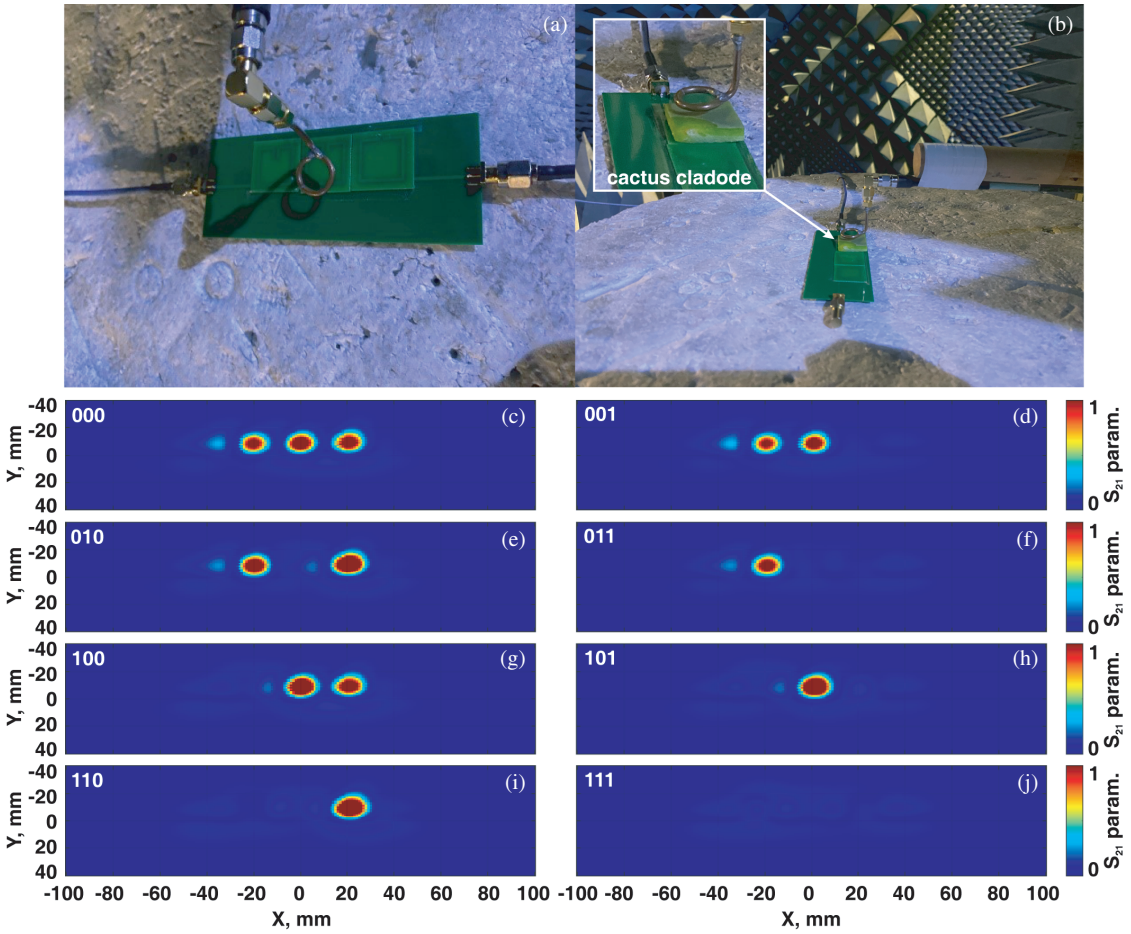

FIGURE 2. Activation of SRR keys with dielectric objects. (a), (b) Photographs of the experimental setup. A near-field magnetic probe is mounted on a moving arm to scan over the devices. Small slices of cactus cladode are placed underneath the SRRs at different locations. (c)–(j) Colormaps of the integrated transmission coefficients between the excitation SMA port and the probe, i.e., $\int |S_{21}(\omega)|d\omega$. Numbers in legends stay for '0'/'1' — dielectric slice absent/present.

Ltd measurement system) and moved 5 mm above the sample to acquire near fields. Three different SRRs (resonant frequencies are 1.35 GHz, 1.45 GHz, and 1.55 GHz) were positioned on the microstrip line. Figs. 2(a) and (b) are the photographs of the experimental arrangement. In this configuration, it is challenging to position fingers beneath the device. For experimental purposes, small slices of cactus (Opuntia ficus-indica) cladode, approximately 1 cm^3 in size and with a high water content similar to that of a human finger, were strategically placed near the SRRs in various combinations. The near-field scan has been performed to verify that the SRRs are activated upon the presence of the cactus slice. A magnetic field probe was mounted on a mechanical scanner, which was moved with 1 mm steps. The diameter of the probe is comparable to the SRR layout, thus the averaged field (the flux through the area of the scanning ring) is picked up. A two-dimensional (2D) scan along the transmission line is performed (Figs. 2(c)–(j)). The second port of the PNA was connected to the probe, and thus S_{21}-parameters were measured. To demonstrate the property of activated keys, the following post-processing was applied. Transmission amplitudes, i.e., $|S_{21}(\omega)|$, were calculated and integrated over the bandwidth — $\int |S_{21}(\omega)|d\omega$. The integration has been performed between 1 GHz and 2 GHz. Figs. 2(c)–(j) demonstrate different combinations of activated keys (SRRs) with the full correlation between the hot spots and the presence of dielectric objects beneath them.

4. SRR KEYS --- FINGER ACTIVATION

After verifying the concept of key activation with a generic dielectric structure and highlighting the SRR-specific field accumulation, the following analysis has been performed to demonstrate that the device can act as a finger-activated touchpad. The key space, in this case, is 8 (2^k, where $k = 3$ is the number of keys). The notations are similar to those used above — '0' stays for an inactivated key, while '1' is when a finger is located above the SRR-activated. For example, $[0, 0, 0]$ is when all SRRs are untouched SRRs. Fig. 3, demonstrating the transmission spectra for different configurations, summarizes the results. In this case, two ports of the calibrated VNA were connected to the transmission line, and the transfer function was measured. The first row is the numerical analysis, where 1 cm^3, $\varepsilon_r = 80$ cube was used for the emulation. CST

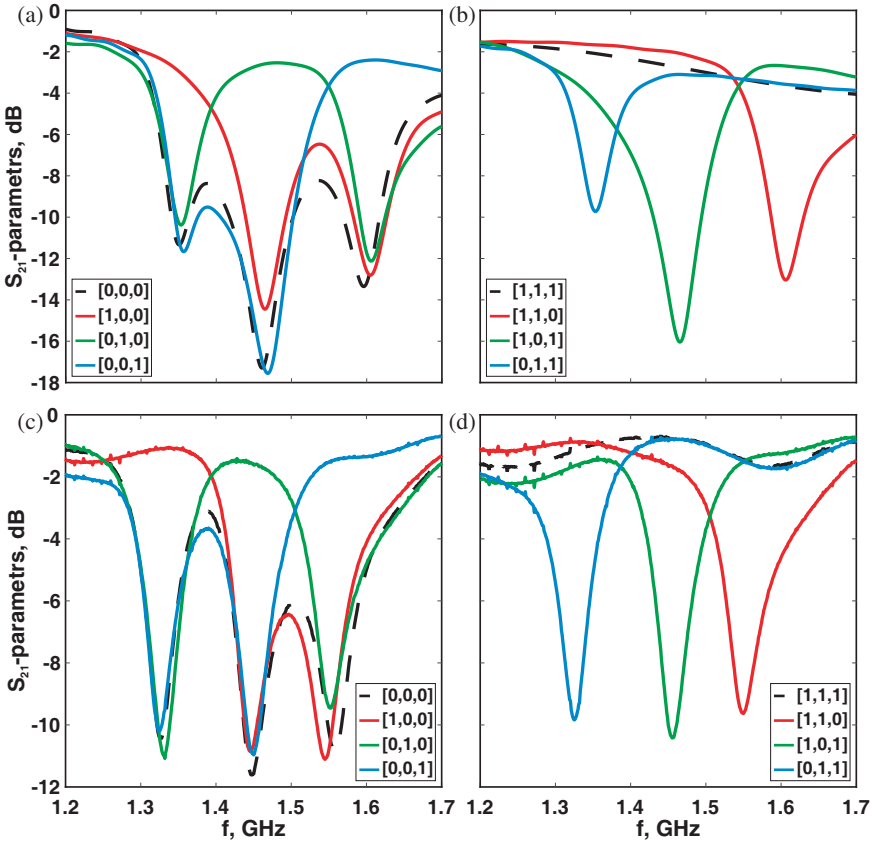

FIGURE 3. Strip line transmission ($|S_{21}|$) in dB for several activation combinations. Legends stay for the configuration. '0' — no finger present, '1' — finger touch. (a), (b) Numerical analysis. (c), (d) Experimental results.

Microwave Studio, Frequency Solver, was used for the modeling. The second row is the experimental data which is found to follow the predictions extremely well. All $2^{k=3}$ combinations were realized and found to be distinguished from each other with very high signal-to-noise ratios (well above 20 dB). 0 bBm was launched through the SMA port. The data below demonstrates that monitoring the transmission at 3 characteristic frequencies, where the SRRs have resonances is sufficient to extract the information reliably. Furthermore, a 10 dB difference in transmission for activated and inactivated cases can relax the demand for calibrating the feeding network, given that it is impedance-matched to the transmission line. Slight difference in the frequency deeps between simulations and experimentally obtained results can be found from Figs. 3(a)–(b) and Figs. 3(c)–(d), respectively. However, it is expected as the simulation model use the closest parameters and characteristics to the experimental sample, but still close to ideal ones.

The research has also considered a set of other SRRs keys combinations and their number in the touchpad that appears in Supplementary 1 for the case of $k = 4$.

5. IMPLEMENTATION OF A LOW-COST STANDALONE SYSTEM

All the characterization in the previous sections was performed with high-grade characterization equipment, i.e., VNA. However, a standalone low-cost device must be developed for practical demonstrations. Here, we demonstrate that a low-grade electronic circuit can control the device and extract the data quite accurately. Fig. 4(a) summarizes the design, which encompasses (i) a voltage control oscillator (VCO) ADF4351, which generates a set of frequencies to match the resonances of the keys; (ii) Power detector (PD) AD8313 operates in the frequency band 0.1–2.5 GHz (in fact, the 1.0–1.7 GHz band is in use) that covers the used key elements' frequency range; (iii) Microchip ATmega328P microcontroller (MCU), interfaced with Arduino-nano board. MCU is connected to VCO via the logic level converter. The exploited Serial Peripheral Interface (SPI) interface allows fast tracking and adjustment of frequencies. The overall hardware cost is $2.5+24+10+1$ USD.

The system operates as follows: at the initial stage, all the SRR keys are assessed, and the transmission through the microstrip is evaluated. This step resembles the measurements with high-grade VNA. Fig. 4(b) demonstrates the row transmission, where 3 SRRs are placed on the microstrip. 3 pronounced dips in the spectrum are clearly seen in this case. After performing this step, the central frequencies, corresponding to the spectral features are stored in the memory, and the monitoring will be performed over the discrete set of frequencies. This approach allows fast data acquisition without a need to perform redundant measurements.

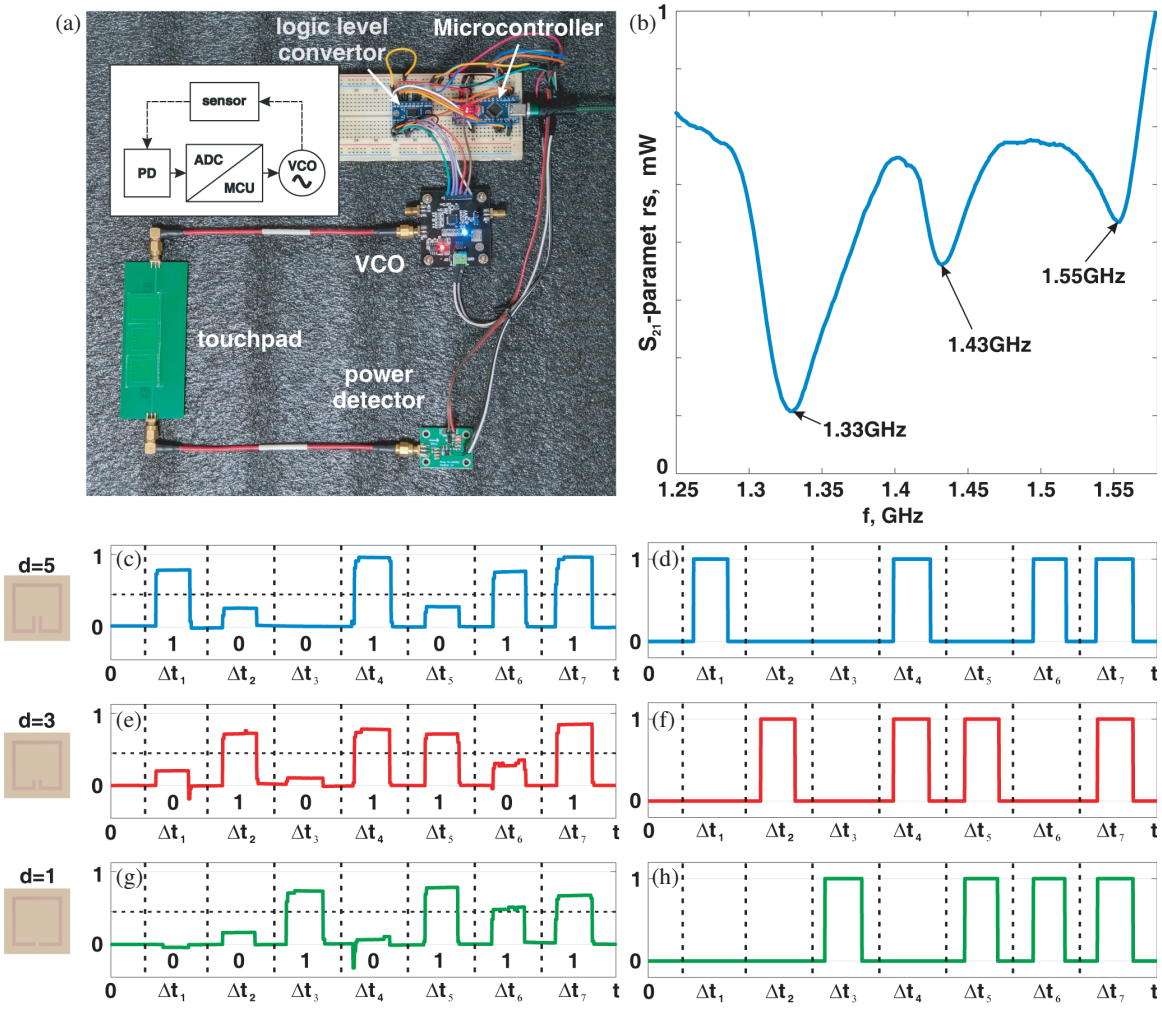

FIGURE 4. (a) Photograph of the low-cost standalone device to monitor the SRR key activation. Key elements are indicated in the legends. Inset — the high-level block diagram of the device. (b) Experimentally retrieved transmission with 3 representative SRRs, positioned on the strip line. (c), (e), and (g) — time sequences of activated and not activated keys — time-dependent power, monitored at representative frequencies (from (b)). (d), (f), and (h) — activation sequences after applying adaptive thresholding on the raw data.

The next step is evaluating the threshold within the analog signal to quantize '0' and '1' levels. Figs. 4(c), (d), and (g) demonstrate time series of activating events for 3 representative keys. The acquisition is done in slots of 500 msec (can be made faster if needed), and the averaged power is recorded. For example, Fig. 4(c) demonstrates the sequence where the key was activated 3 times. Owing to noise and lack of synchronization (this is indeed the case in random activation of the keys in practice), the energy levels can vary between minimum and maximum. Hence, the adoptive thresholding must be set. Fig. 4(d) demonstrates the result. All other keys underwent a similar procedure — panels (f) and (h), for example.

The device operability in real time can be found in Supplementary 2 and 3 as video records with representation of time sequences of three and four SRRs keys combinations activation, similar to that shown in Figs. 4(c)–(d). Additionally, a buzzer was mounted on the board for sound reproducing that one can found on the video records of the Supplementary 2 and 3.

Supplementary 4 demonstrates a possibility of the complete standalone usage of the device. We show the option of the device operability with battery power supply.

6. CONCLUSION

In conclusion, an application of Split Ring Resonators (SRRs) in creating highly responsive, touchless key activation systems was explored. 14 SRRs with distinctive resonances within the 1.0–1.7 GHz frequency range were designed and demonstrated. Specifically, a single geometrical parameter was found to grant a high level of tunability thus making the analysis and manufacturing straightforward. The resonators were integrated on a microstrip line, altering the transmission coefficient predictably as influenced by external dielectric perturbations, such as human hands or a phantom dielectric object. After showing how keys can be independently monitored through spectral sharing, a low-cost device to manage this setup has been successfully demonstrated. This setup not only replicated the highly ac-

curate characterization achieved with sophisticated equipment like vector network analyzers, but also demonstrated the potential to scale this technology for broader applications. In these settings, expensive, high-grade equipment could be replaced with cheaper, yet sufficiently reliable alternatives.

ACKNOWLEDGEMENT

V. B., M. K., V. T., and D. V. acknowledge the support from the RRF project Latvian Quantum Technologies Initiative Nr. 2.3.1.1.i.0/1/22/I/CFLA/001.

REFERENCES

[1] Findlater, L. and J. O. Wobbrock, "From plastic to pixels: In search of touch-typing touchscreen keyboards," *Interactions*, Vol. 19, No. 3, 44–49, May 2012.

[2] Pickering, J. A., "Touch-sensitive screens: The technologies and their application," *International Journal of Man-Machine Studies*, Vol. 25, No. 3, 249–269, Sep. 1986.

[3] Ouyang, C., D. Liu, K. He, and J. Kang, "Recent advances in touch sensors for flexible displays," *IEEE Open Journal of Nanotechnology*, Vol. 4, 36–46, 2022.

[4] Anwer, A. H., N. Khan, M. Z. Ansari, S.-S. Baek, H. Yi, S. Kim, S. M. Noh, and C. Jeong, "Recent advances in touch sensors for flexible wearable devices," *Sensors*, Vol. 22, No. 12, 4460, Jun. 2022.

[5] Kwon, O.-K., J.-S. An, and S.-K. Hong, "Capacitive touch systems with styli for touch sensors: A review," *IEEE Sensors Journal*, Vol. 18, No. 12, 4832–4846, Jun. 2018.

[6] Kang, M., J. Kim, B. Jang, Y. Chae, J.-H. Kim, and J.-H. Ahn, "Graphene-based three-dimensional capacitive touch sensor for wearable electronics," *ACS Nano*, Vol. 11, No. 8, 7950–7957, Aug. 2017.

[7] Kim, H.-K., S. Lee, and K.-S. Yun, "Capacitive tactile sensor array for touch screen application," *Sensors and Actuators A: Physical*, Vol. 165, No. 1, 2–7, Jan. 2011.

[8] Cooper, C. B., K. Arutselvan, Y. Liu, D. Armstrong, Y. Lin, M. R. Khan, J. Genzer, and M. D. Dickey, "Stretchable capacitive sensors of torsion, strain, and touch using double helix liquid metal fibers," *Advanced Functional Materials*, Vol. 27, No. 20, 1605630, May 2017.

[9] Sarwar, M. S., R. Ishizaki, K. Morton, C. Preston, T. Nguyen, X. Fan, B. Dupont, L. Hogarth, T. Yoshiike, R. Qiu, *et al.*, "Touch, press and stroke: A soft capacitive sensor skin," *Scientific Reports*, Vol. 13, No. 1, 17390, Oct. 2023.

[10] Lee, C.-J., J. K. Park, C. Piao, H.-E. Seo, J. Choi, and J.-H. Chun, "Mutual capacitive sensing touch screen controller for ultrathin display with extended signal passband using negative capacitance," *Sensors*, Vol. 18, No. 11, 3637, Oct. 2018.

[11] Boybay, M. S. and O. M. Ramahi, "Material characterization using complementary split-ring resonators," *IEEE Transactions on Instrumentation and Measurement*, Vol. 61, No. 11, 3039–3046, 2012.

[12] Movchan, A. B. and S. Guenneau, "Split-ring resonators and localized modes," *Physical Review B — Condensed Matter and Materials Physics*, Vol. 70, No. 12, 125116, Sep. 2004.

[13] Naqui, J., L. Su, J. Mata, and F. Martín, "Recent advances in the modeling of transmission lines loaded with split ring resonators," *International Journal of Antennas and Propagation*, Vol. 2015, No. 1, 792750, 2015.

[14] García-García, J., F. Martín, J. D. Baena, R. Marqués, and L. Jelinek, "On the resonances and polarizabilities of split ring resonators," *Journal of Applied Physics*, Vol. 98, No. 3, 033103, Aug. 2005.

[15] Hao, X., Y. Chen, M. Liu, X. Min, X. Cheng, Q. Wang, Q. Xu, X. Zhang, and J. Han, "Recent advances in terahertz manipulations using C-shape-split-ring-resonator metasurfaces," *Advanced Optical Materials*, Vol. 12, No. 15, 2302975, May 2024.

[16] Moser, H. O., B. D. F. Casse, O. Wilhelmi, and B. T. Saw, "Terahertz response of a microfabricated rod–split-ring-resonator electromagnetic metamaterial," *Physical Review Letters*, Vol. 94, No. 6, 063901, Feb. 2005.

[17] Vovchuk, D., M. Khobzei, and M. Khavruniak, "Sensing properties of SRR: Influence of finger touching," in *2019 IEEE International Scientific-Practical Conference Problems of Infocommunications, Science and Technology (PIC S&T)*, 799–802, Kyiv, Ukraine, Oct. 2019.

[18] Liu, W., H. Sun, and L. Xu, "A microwave method for dielectric characterization measurement of small liquids using a metamaterial-based sensor," *Sensors*, Vol. 18, No. 5, 1438, 2018.

[19] Puentes, M., M. Schüßler, and R. Jakoby, "2D sensor array based on split ring resonators for monitoring of organic tissue," in *SENSORS, 2011 IEEE*, 272–275, Limerick, Ireland, Oct. 2011.

[20] Ebrahimi, A., W. Withayachumnankul, S. Al-Sarawi, and D. Abbott, "High-sensitivity metamaterial-inspired sensor for microfluidic dielectric characterization," *IEEE Sensors Journal*, Vol. 14, No. 5, 1345–1351, 2014.

[21] Choi, S., S. Eom, M. M. Tentzeris, and S. Lim, "Inkjet-printed electromagnet-based touchpad using spiral resonators," *Journal of Microelectromechanical Systems*, Vol. 25, No. 5, 947–953, Oct. 2016.

[22] Memon, M. U., A. Salim, H. Jeong, and S. Lim, "Metamaterial inspired radio frequency-based touchpad sensor system," *IEEE Transactions on Instrumentation and Measurement*, Vol. 69, No. 4, 1344–1352, Apr. 2020.

[23] Nikitin, P., "Leon Theremin (Lev Termen)," *IEEE Antennas and Propagation Magazine*, Vol. 54, No. 5, 252–257, 2012.

[24] Mathew, K., "The evolution of the theremin," Capstone Projects and Master's Theses, California State Univ California State University, Monterey Bay, CA, USA, May 2019.

[25] Skeldon, K. D., L. M. Reid, V. McInally, B. Dougan, and C. Fulton, "Physics of the theremin," *American Journal of Physics*, Vol. 66, No. 11, 945–955, Nov. 1998.

[26] Capolino, F., *Applications of Metamaterials*, CRC Press, 2017.

[27] Harnsoongnoen, S., "Microwave sensors based on coplanar waveguide loaded with split ring resonators: A review," *KMUTNB International Journal of Applied Science and Technology*, Vol. 12, No. 4, 224–234, 2018.